INTERNATIONAL JOURNAL OF GREEN ENERGY
2020, VOL. 17, NO. 13, 884–893
https://doi.org/10.1080/15435075.2020.1809427

Taylor & Francis
Taylor & Francis Group

Performance Enhancement of a Beta Type Rhombic Drive Stirling engine

Can Cinar[a], Hamit Solmaz[a], Duygu Ipci[a], Emre Yılmaz[b], and Fatih Aksoy[c]

[a]Faculty of Technology, Department of Automotive Engineering Teknikokullar, Gazi University, Ankara, Turkey; [b]Arifiye Vocational High School, Sakarya University of Applied Sciences, Sakarya, Turkey; [c]Faculty of Technology, Department of Automotive Engineering, Afyon Kocatepe University, Afyon, Turkey

ABSTRACT

Stirling engines maintain attraction because of their high energy conversion efficiencies. In this study, experimental comparison of a beta-type Stirling engine for two different rhombic-drive mechanisms was presented. In one of the rhombic mechanisms, spur gears were used and the gear shaft was supported in bearings from one side. In the other mechanism, two helical gears were placed on crankshafts and the crankshafts were supported in bearings from both sides. Rhombus lengths of the mechanisms were determined as 66 mm and 80 mm to provide same constant compression ratio of 2.5 for both configurations. Both mechanisms were used in the same beta-type Stirling engine having same cylinder, piston and displacer dimensions. Performance parameters of the engines were evaluated at different helium charge pressures (2–4 bar) and hot-end temperatures (400–600°C). The hot-end of the displacer cylinder was heated by a liquefied petroleum gas (LPG) burner. The engine power increased by 132%, friction losses and gear noses were reduced by supporting the rhombic-drive mechanism from both side and using helical gears. The maximum output torque and power of the engine were obtained as 13.14 Nm at 428 rpm engine speed and 663 W at 800 rpm engine speed, respectively, at 600°C hot-end temperature and 4 bar charge pressure.

ARTICLE HISTORY
Received 23 May 2020
Accepted 25 July 2020

KEYWORDS
Rhombic-drive mechanism; stirling engine; engine performance; bearing; reducing friction

1. Introduction

The demand for energy is increasing in parallel to the human population over world and the developing digital technology. Another fact is that most of the energy needs are still supplied from fossil-based fuels. The main drawback of the fossil fuels is their harmful aspects on the environment. It is predicted that the nearest chaos that threatens the world will be climate change caused by global warming (Ahima 2020; Bergquist and Warshaw 2019; Choi, Gao, and Jiang 2020; Owusu and Asumadu-Sarkodie 2016). Atmospheric level of the carbon dioxide (CO_2), which is a key factor to track the trend of the global warming, exceeded 400 ppm permanently in 2016. This is a critical dam for CO_2 because 450 ppm is the maximum level that committed to keep the global temperature rise below 2 °C (Başaran 2020; Bratspies 2018; Moulton and Silverwood 2018; Wigley 2018; Wigley et al. 2009). Due to these concerns and the rapid depletion of the fossil-based fuels, utilization of the renewable energy sources are becoming mandatory day by day. The replacement of fossil-based fuels with renewable energy sources to compensate the energy demand also reduces the dependency of the countries to other supplier countries in terms of energy. That makes renewable energy sources more attractive for the politics as well (Ansari et al. 2016; Menegaki 2008; Poorghasemi et al. 2017). For this reason, researchers focused on renewable energy sources such as alternative fuels (Ciniviz, Örs, and Kul 2017; Özsezen 2017; Sezer 2019; Uyumaz et al. 2017), geothermal (García-Gil et al. 2020; Olabi et al. 2020; Paulillo et al. 2020), solar (Gong, Li, and Wasielewski 2019; Ma and Wang 2020; Tilley 2019), tidal (Auguste et al. 2019; El Tawil et al. 2019), wind etc. (Katopodis et al. 2019; Lundie et al. 2019; Wang et al. 2019).

Alternative fuel technologies takes a great attention during the last decades because of their capability to reduce CO2 resulted from internal combustion engines which is powered by fossil-based fuels. Biodiesel is an alternative fuel produced by both edible and nonedible vegetable oils. Biodiesel seems to be a proper alternative to diesel fuel for compression ignition engines (Can et al. 2016; Çelikten, Mutlu, and Solmaz 2012; Uyumaz 2020). However, its high viscosity do not allow to use pure biodiesel on advanced compression ignition engines utilizing common rail technologies. Also, biodiesel threats the edible oil food stock. Alcohol fuels, especially ethanol, is utilized generally as an alternative fuel for spark ignition engines because of its high octane rating (Ardebili, Solmaz, and Mostafaei 2019; Ardebili et al. 2020; Solmaz 2020). However, conventional internal combustion engines have a limited thermal energy conversion rate in a range of 25–42%. Advanced low temperature combustion modes provide high thermal efficiency and low exhaust emissions together (Calam 2020; Calam et al. 2019; Polat et al. 2020a, 2020b). However, these technologies don't proper to use for industrial energy production because they are still in development progress. Therefore, to reduce the release of the greenhouse gas of CO2 to environment, the high energy conversion devices capable to use renewable sources are required.

Stirling engines are capable to produce power with high effective energy conversion rate (Solmaz and Karabulut 2014). Stirling engines are attractive devices because of their

CONTACT Hamit Solmaz hsolmaz@gazi.edu.tr Faculty of Technology, Department of Automotive Engineering Teknikokullar, Gazi University, Ankara, Turkey

high thermal efficiency, which is equal to carnot cycle efficiency for a regenerative Stirling engine in theory. Besides, many kinds of energy sources such as, solar, nuclear, biomass and geothermal energies and different types of fossil-based fuels could be used in Stirling engines due to external heating (Wang et al. 2016; Kongtragool and Wongwises; Caetano et al. 2019; Al Moussawi, Fardoun, and Louahlia-Gualous 2016; Chahartaghi and Sheykhi 2019; Güven, Bedir, and Anlaş 2019). Among these sources, solar energy stands out because of its features as cost effective and infinitive energy potential. Solar energy can be converted to electricity by means of photovoltaic technologies, Stirling engines, solar towers, concentrated solar technologies etc. Energy conversion efficiency of the photovoltaics, which are widely used to produce electricity from the sun, are about 15–20%. The maximum energy conversion efficiency is reach almost 23% for an excessively expensive photovoltaic system (Benato and Stoppato 2019; Cui et al. 2019; Febriansyah et al. 2019; Teo, Lee, and Hawlader 2012). The solar dish/Stirling engine system is the most efficient energy conversion system for electricity production (Beltrán-Chacon et al. 2015). Solar to electricity conversion efficiency for the Stirling engines are reported about 40% (Bosshard et al. 2006).

In the kinematic Stirling engines power generation is provided by the synchronized motion of the piston and displacer by means of a drive mechanism (Erol, Yaman, and Doğan 2017; Kongtragool and Wongwises 2003). Crank drive (Erol, Yaman, and Doğan 2017), rhombic drive (Alfarawi 2020; Badr et al. 2016), scotch yoke (Erol, Yaman, and Doğan 2017; Sripakagorn and Srikam 2011), ross yoke (Bataineh 2018), and swashplate (Pogulyaev, Nikishin, and Zheltov 2017) are the main drive mechanisms that used often in Stirling engines. It was reported that the rhombic-drive beta-type Stirling engines has a higher specific power output compared to other drive mechanisms and cylinder configurations (Alfarawi 2020; Ardebili, Solmaz, and Mostafaei 2019). R.J. Meijer firstly used rhombic-drive mechanism for a beta-type Stirling engine in 1953 (Cheng, Huang, and Yang 2019; Gultekin, Cinar, and Okur 2020). Rhombic-drive mechanism are used for beta-type Stirling engines. Displacer and power piston are placed in the same cylinder in beta configuration. Displacer rod extends in the power piston and both displacer and power piston operates in same axis that reduces lubrication need. Besides, there is no side for acting on neither power piston nor displacer. Thus, mechanical losses are minimized between piston and cylinder surface (Ardebili, Solmaz, and Mostafaei 2019; Cheng, Huang, and Yang 2019; Cheng and Yu 2012).

A lot of research are focused on beta-type Stirling engines due to provide higher power density and compact design (Ahmed et al. 2019; Cheng and Yang 2012; Yang, Cheng, and Huang 2018). Shendage, Kedare, and Bapat (2011) designed and analyzed a rhombic-drive mechanism for a beta-type Stirling engine. They presented the design methodology to optimize the phase angle for the beta-type Stirling engine. Babaelahi and Sayyaadi (2016) developed a second-order numerical method to simulate the GPU-3 Stirling engine. Alfarawi (2020), conducted a numerical study to compare the performance of the rhombic-driven and crank-driven beta-type Stirling engines. A nonideal thermodynamic model was used in analysis. It was reported that the rhombic-drive Stirling engine provided 32% higher engine power and 20% higher thermal efficiency compared to crank-drive Stirling engine. The low power density of the crank-drive stirling mechanism was caused by increasing hysteresis pumping loses at high engine speeds. Sripakagorn and Srikam (2011) presented the design and performance results of a beta-type Stirling engine operating at average temperature differences. An electrical heater was used to test the engine. The engine produced 95.4 W shaft power at 360 rpm engine speed, 500°C hot-end temperature and charge pressure of 7 bar. At maximum power condition, 9.35% thermal efficiency was reported. Cheng, Yang, and Keong (2013) carried out both theoretical and experimental study to estimate performance of a beta-type Stirling engine having a rhombic-drive mechanism. The engine produced 390 W shaft power with 32.2 % thermal efficiency at 1400 rpm engine speed at a charge pressure of 8 bar e and heating temperature of 850°C using an electrical heater. In an experimental study, Cinar, Aksoy, and Okur (2013) manufactured and tested a beta-type Stirling engine having a rhombic-drive mechanism. The performance tests of the engine were conducted by using a LPG burner. Air and helium were used as working fluid. The engine provided a maximum power of 95.77 W at engine speed of 575 rpm, hot end temperature of 450°C and charge pressure of 2 bar helium. Karabulut et al. (2009) designed a displacer driving mechanism controlled by a lever to perform a better approach to the theoretical Stirling cycle. Maximum power output was obtained as 51.93 W at engine speed of 453 rpm, charge pressure of 2.8 bar and hot end temperature of 200°C. They obtained about 50% higher power by using slotted displacer cylinder having 214% larger inner surface compared to smooth cylinder. Abdullah, Yousif, and Sopian (2005) designed a low temperature difference Stirling engine. The engine was considered as double acting. The crankshaft of the engine was supported by nylon bushes to reduce friction. The maximum power output of the engine was calculated about 350 W. However, the effects of the nylon bushes on the power gain did not presented in the study. Masser et al. (2020) presented a numerical study optimizing the motion of the piston to increase the engine performance. The regenerator was assumed and modeled as an ideal regenerator. It was found that the optimized piston motion enhances the engine thermodynamics and the power output increased about 50%.

In this study, performance of a beta-type Stirling engine with two different rhombic mechanisms was investigated experimentally. The rhombic mechanisms have different types of gears, bearings and rhombus lengths. Better performance characteristics were obtained with the rhombic mechanism with double-sided bearing and helical gear. The tests were conducted at displacer cylinder hot-end temperatures of 400°C, 500°C and 600°C using helium as the working fluid at 2–4 bar charge pressures.

2. Material and methods

2.1. Design and manufacturing of the test engine

In this paper, two different rhombic-drive mechanisms were manufactured and tested for the same beta-type Stirling

engine. The schematic view of the prototype beta-type Stirling engine is shown in Figure 1. The manufacturing details of the engine were given in Reference (Aksoy et al. 2017). In the Stirling engine, both the displacer piston and the displacer cylinder were made of ASTM 304 steel and the displacer gap was left 0.7 mm. This gap between the displacer and the cylinder enables the gas flow between hot space and cold space.

In Figure 1 gear pin was indicated with red joint and the working process of the engine were explained movement of gear pin to positions of A, B, C, and D symbols. During the gear pin moves from A to B, power piston position remains almost the same location and the displacer moves downward. Thus, the total volume remains constant. At this process, the working fluid flows from the cold volume to hot volume by performing heating process at a constant temperature. When the gear pin moves from B to C, power piston and displacer move to bottom of the cylinder with same rate. So, the cold volume remains constant and hot volume expands. The work generates as a result of the expansion of the hot volume. While the gear pin moves from C to D, power piston position remains at the same location and displacer moves upward. The working fluid moves from hot volume to cold volume at a constant volume and the cooling process carry out. When the gear pin moves from D to A, power piston and displacer move to top dead center. The working fluid flows to from hot volume to cold volume and the fluid is compressed in cold volume.

The displacer cylinder inner surface was extended with the axial slots of 3 mm depth and 1.5 mm width as shown in Figure 2. 1200 cm^2 heat transfer area were provided inside the displacer cylinder with this enlargement. As shown in Figure 3, a LPG burner was used to heat the upper external surface of the displacer cylinder. In the LPG burner, air and LPG flows were controlled via a computer controlled flow meter to set the hot

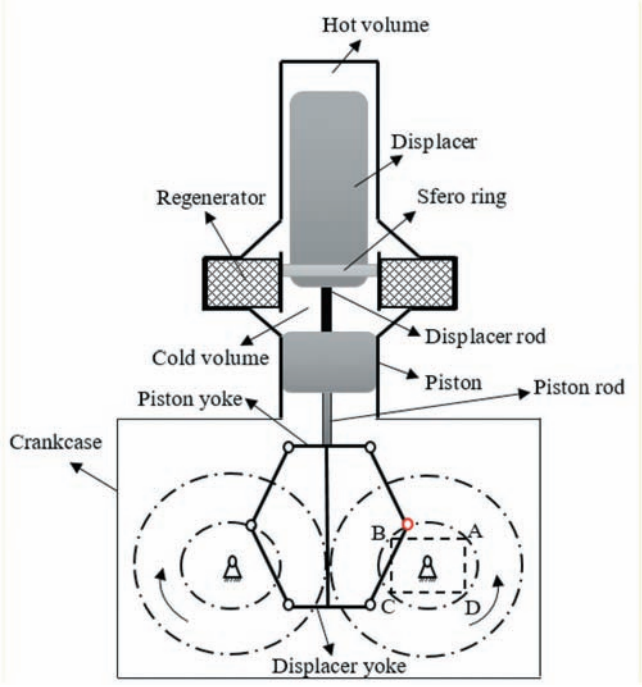

Figure 1. Schematic view of the test engine.

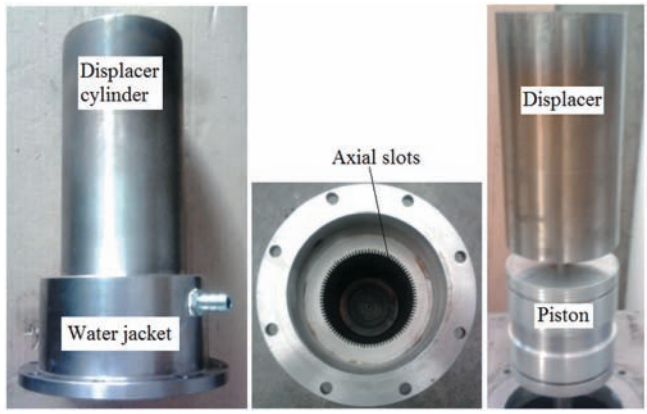

Figure 2. Displacer, displacer cylinder and piston of the engine.

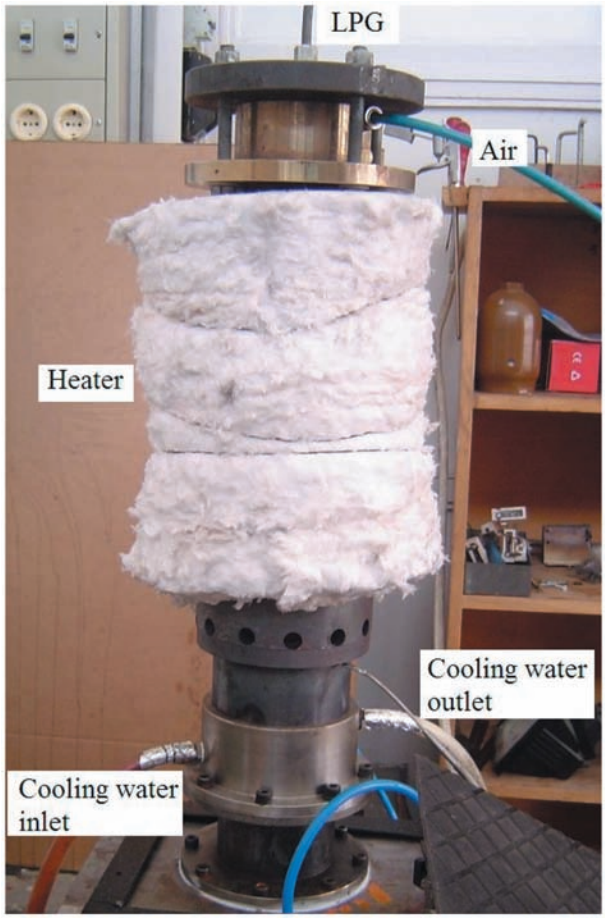

Figure 3. Photograph of the LPG heater.

end temperature of the displacer cylinder to a certain value. A water jacked was placed on the cold side external surface of the displacer cylinder. The cold side of the displacer cylinder external surface was cooled by means of water circulation. The power piston was made of aluminum alloy. The piston cylinder was made of oil hardened steel and the inner surface of the cylinder liner was finished by grinding. Technical details of the test engine are given in Table 1.

In the present study, two different rhombic mechanisms were compared by means of engine performance. In order to

Table 1. Technical specifications of the test engine (Aksoy et al. 2017; Cinar 2014).

Parameters	Specification	
Engine type	Beta	
Diameter of the displacer cylinder [mm]	86	
Diameter of the displacer rod [mm]	18	
Diameter of the piston [mm]	86	
Hot end temperature [K]	673–873	
Cold end temperature [K]	298	
Working fluid	Helium	
Charge pressure [bar]	2–4	
Driving mechanism	Rhombic (spur gears)	Rhombic (helical gears)
Rhombus length [mm]	66	80
Length of displacer [mm]	155	155
Length of displacer rod [mm]	322	361
Length of piston [mm]	90	77
Length of piston rod [mm]	100	124
Compression ratio	2.5	2.5

Table 2. Uncertainties of the calculated values and accuracies of the test equipments.

Parameter	Accuracy	Uncertainty
Engine Speed [rpm]	±1	-
Temperature [°C]	±1.5	-
Torque [Nm]	±0.05 kg [load cell accuracy]	±0.017
Power [W]	-	0.3%-0.7%
Charge pressure [bar]	±0.01	-

perform a reliable comparison, the same cylinder, piston and displacer were used in both of the engines. Thus, cooler and heater heat transfer surface areas, heater and cooler volumes were kept constant in comparison. However, the compression ratio is another important parameter affecting the Stirling engine performance. In order to compare the performance of the mechanisms at same compression ratio, rhombus lengths of the two mechanisms were determined as 66 mm and 80 mm. The compression ratio of the both configurations was calculated as 2.5.

In the first mechanism, spur gears were used and the gear shafts were supported in bearings from one sides (Figure 4a). During the tests, the increase in the charge pressure pushed the gears through the bearings and caused to increase the friction losses. To eliminate the disadvantages of using spur gears and bearing the mechanism from only one side, a new rhombic-drive mechanism was designed and manufactured (Figure 4b). In the mechanism, two equal size crankshafts were supported in bearings from both side with roll bearings. Instead of spur gears, two helical gears rotate in opposite directions were placed on the crankshafts.

2.2. Experimental setup and testing procedure

The schematic illustration of the experimental setup is given in Figure 5. A prony-type engine test bed was used in the experiments. Engine load was measured using a strain gauge load cell sensor with a brand name of ESIT BB20 having 0.003 Nm accuracy. The engine speed was measured by a digital tachometer with a brand name of ENDA ETS1410, with an accuracy of 1 rpm. Hot-end and cold-end temperatures were measured using a multi-point electronic temperature indicator, ELIMKO-6000, with 1°C accuracy. NiCr–Ni (Type K) thermocouples that can measure up to 1200°C were used. A digital manometer with a 0.01 bar accuracy was used to measure the charge pressure. The helium charge pressure inside the engine block was regulated using a pressure regulation valve. The uncertainties of the calculated parameters and the accuracies of the test equipment are presented in Table 2.

The upper surface of the displacer cylinder named as hot-end was heated by an LPG heater. During the tests, the charge pressure inside the engine block was set to any desired value and then by regulating air and LPG flows the temperature of the hot-end was adjusted to the determined value. Air and LPG flows were controlled via a computer controlled flow meter. The performance tests were conducted at 400°C, 500°C and 600°C hot-end temperatures and 2–4 bars helium charge pressures. The displacer cylinder lower side and the piston liner outer surface were cooled by circulating water. The outlet temperature of the water was kept at about 25°C. At each hot-end temperature level, helium charge pressure was increased gradually up to the power declines. At each hot-end temperature and charge pressure, the engine torque was set to any value by varying the braking force of the dynamometer. Output power was calculated for each measured value of torque and speed. The test results were given as speed-torque and speed-power variations for each hot-end temperature and charge pressure values.

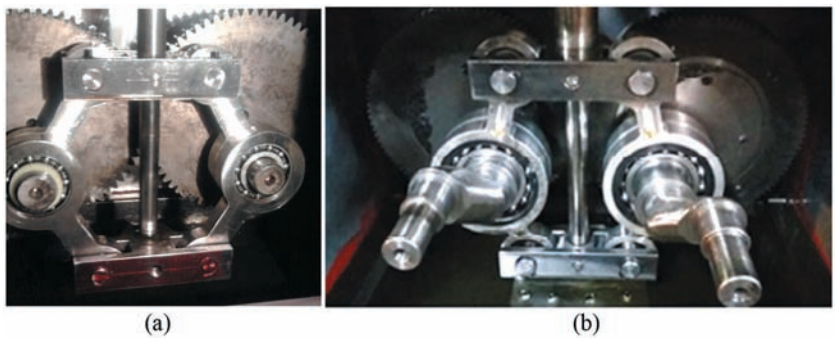

Figure 4. Two different rhombic-drive mechanisms.

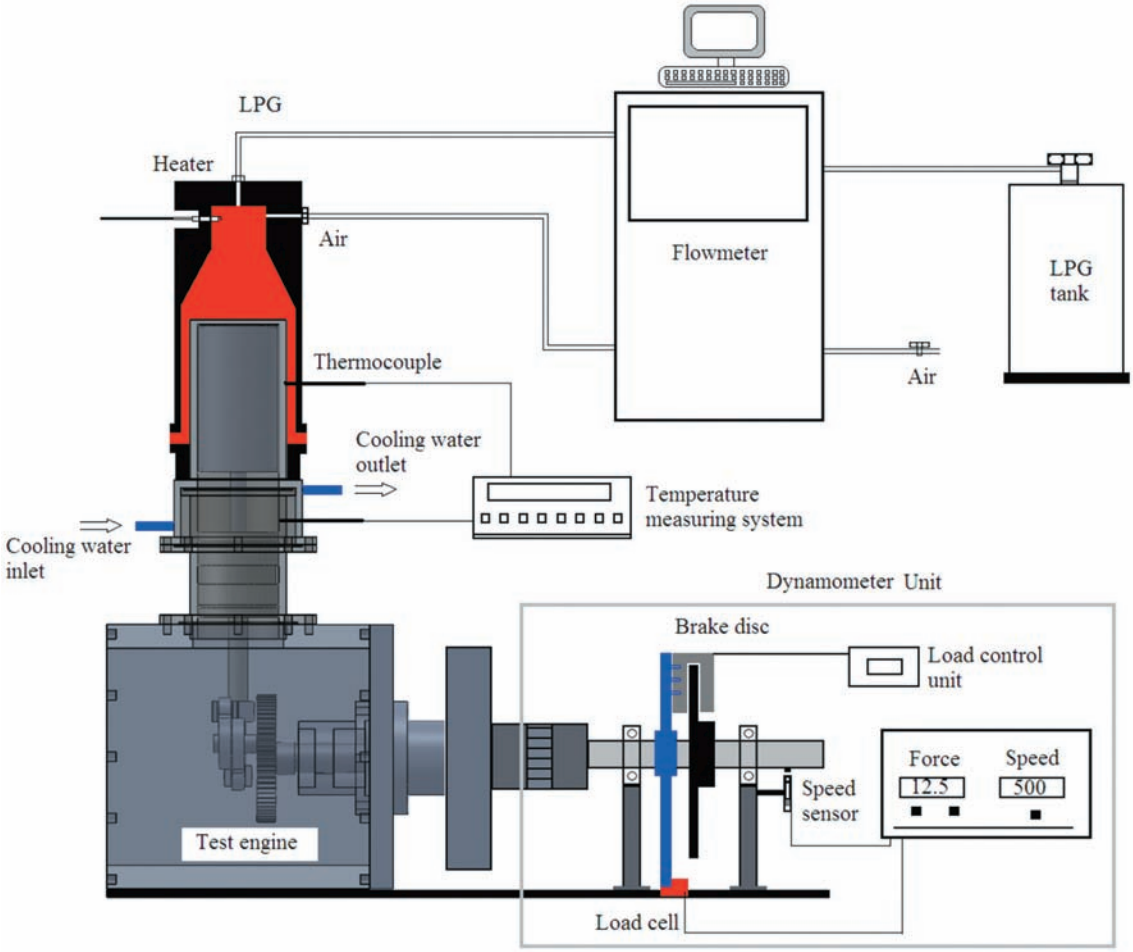

Figure 5. Schematic illustration of the experimental setup.

3. Results and discussion

In the experiments, torque and power variations were obtained with engine speed for different charge pressures and hot end temperatures, for two different rhombic-drive mechanisms. The rhombic mechanism supported with only one sided bearing was illustrated with dashed line while the solid line shows the results of the rhombic mechanism having two sided bearing. The variations of engine torque with engine speed at 400°C, 500°C, and 600°C hot-end temperatures are given in Figs. 6–8. At high engine speeds, the time interval required for heat transfer from the heater surface to working fluid decreases considerably. Therefore, Stirling engine provides maximum effective engine torque at lower engine speeds. As it is seen on figures, maximum engine torques corresponding to 400°C, 500°C and 600°C hot-end temperatures were obtained as 6.93 Nm at 290 rpm, 9.35 Nm at 350 rpm and 13.14 Nm at 428 rpm, respectively. For 400°C hot-end temperature, maximum engine torque was obtained at 3 bar charge pressure. With the increase of hot-end temperature, maximum torques were obtained at 4 bar charge pressure for 500°C and 600°C (Figs. 7 and 8). The torque increases with decrease of the engine speed. Due to decrease in the heat transfer to the working fluid and increase of friction losses, engine torque decreases with the increase of engine speed.

As shown in Figs. 6–8, about 3 times more engine torque was obtained with the rhombic-drive mechanism having 80 mm rhombus length. The compression ratio is a dominant factor affecting the engine torque and thermal efficiency. If the sufficient heating can be provided for working fluid, as the compression ratio is rising, an increase in engine torque is expected. In the present study, the compression ratios of the both engine configurations were equal. Therefore, it can be said that the enhancement in the engine torque does not depend on the engine parameters such as compression ratio. In the configuration of 80 mm rhombus length, helical gears were used and the crankshaft was supported in bearings from both side with roll bearings. Therefore, engine torque was significantly increased with the decrease of friction losses. The maximum engine torque was obtained as 4.56 Nm at 400 rpm engine speed for 66 mm rhombus length mechanism at 4 bar charge pressure and 600°C hot-end temperature. At the same charge pressure and hot-end temperature, 2.88 times more engine torque was obtained as 13.14 Nm at 428 rpm for 80 mm rhombus length mechanism. Masser et al. (2020) presented that the engine performance could be increased by optimizing the motion of the power piston. An optimizied piston motion may reduce the flow losses, improve the heat transfer (Masser et al. 2020). The increase of engine torque in case of using 80 mm rhombus length configuration might also have resulted

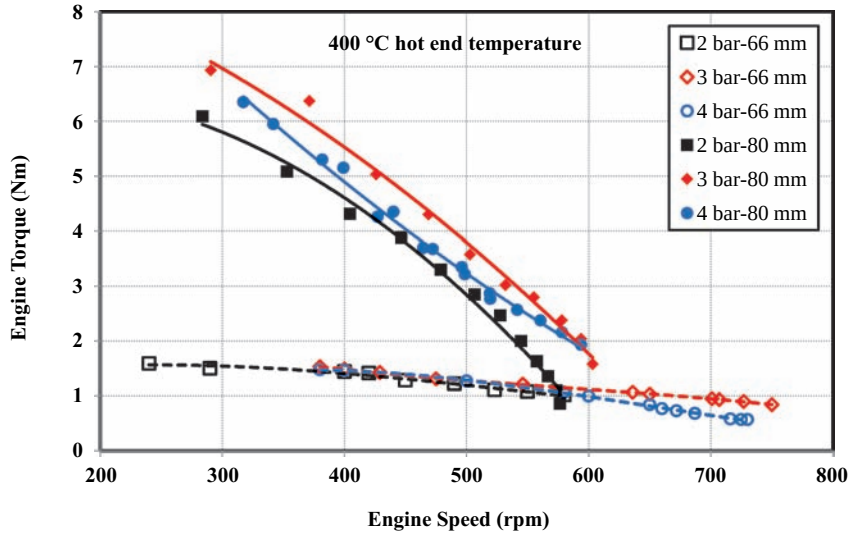

Figure 6. Variation of engine torque with engine speed at 400°C.

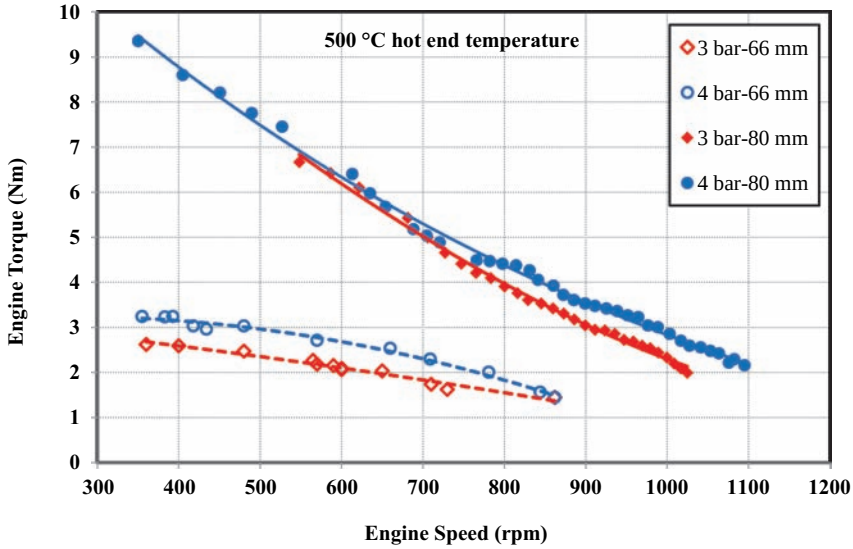

Figure 7. Variation of engine torque with engine speed at 500°C.

because of the changed piston motion compared to the engine configuration of 66 mm rhombus length.

The variations of engine power with engine speed at 400°C, 500°C and 600°C hot-end temperatures are given in Figs. 9–11. Maximum engine powers were obtained as 248 W at 371 rpm, 411 W at 527 rpm and 663 W at 800 rpm engine speeds at the hot end temperatures of 400°C, 500°C and 600°C, respectively. As shown in Figure 9, maximum engine powers were obtained at 3 bar charge pressure for two different rhombic-drive mechanisms at 400°C hot end temperature. As the hot end temperatures increased to 500°C and 600°C, the optimum charge pressure also increased to 4 bar charge pressure.

At 600°C hot end temperature, maximum engine power was obtained as 663 W at 800 rpm engine speed with the engine having 80 mm rhombus length. Due to higher friction losses of the rhombic-drive mechanism, engine power decreased by 132% with the engine having 66 mm rhombus length. Maximum engine power was obtained as 285 W at 685 rpm engine speed with the engine having 66 mm rhombus length. In the present study, flow rate of the LPG was not measured. Therefore, it is not possible to present exact efficiency values for different operating conditions but, for the same hot end temperature and the charge pressure, obtaining higher power output also indicated that the engine thermal efficiency was increased for the engine configuration of 80 mm rhombus length.

The variation of maximum engine torque and power with hot-end temperature is shown in Figure 12. The curves indicate that an increase in hot-end temperature causes an increase in engine torque and power with two rhombic-drive mechanism. The maximum engine torque and power depend on the parameters such as heat transfer surface area of both heater and cooler, specific heat of the working fluid, the mass of the working fluid charged into engine, charge pressure, pressure loss in regenerator area etc. In the present study two different rhombic mechanism was used for same power and displacer cylinder. Thus, in both

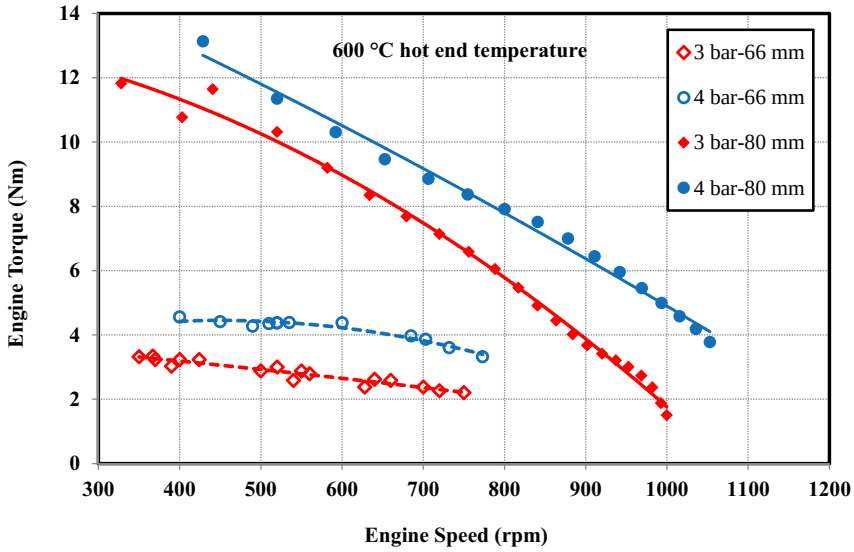

Figure 8. Variation of engine torque with engine speed at 600°C.

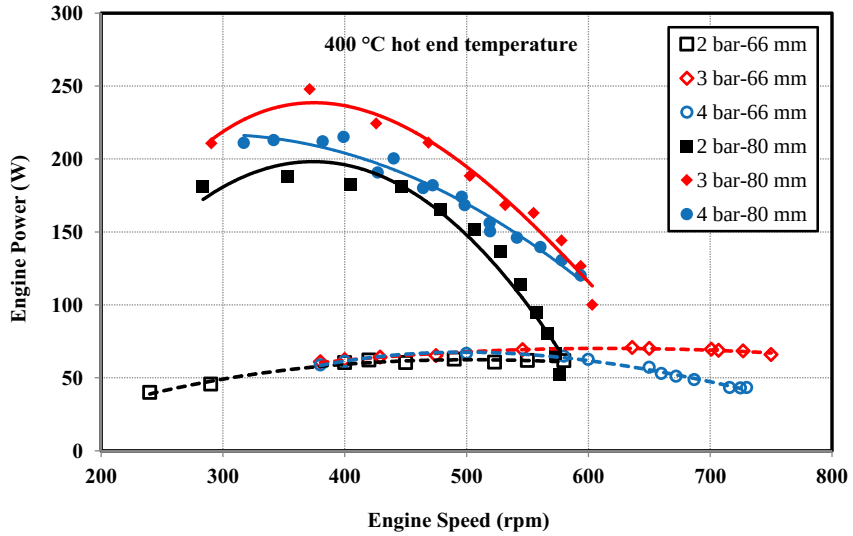

Figure 9. Variation of engine power with engine speed at 400°C.

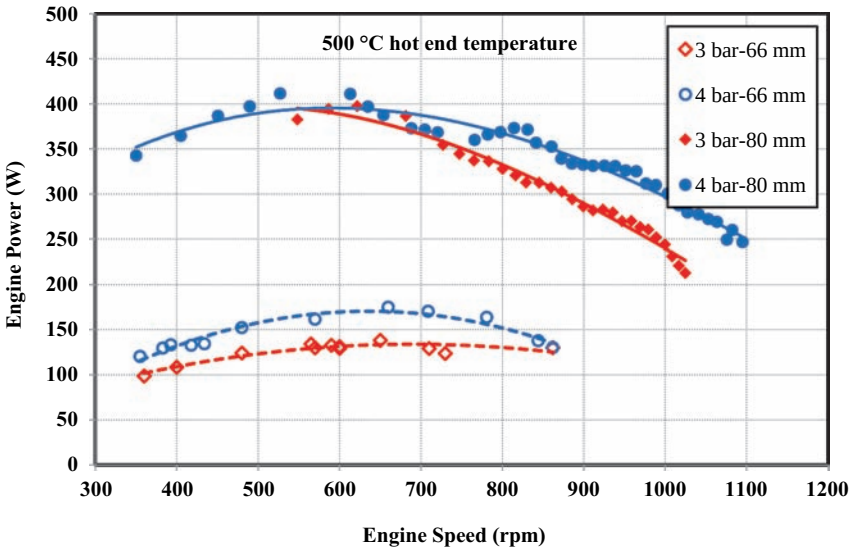

Figure 10. Variation of engine power with engine speed at 500°C.

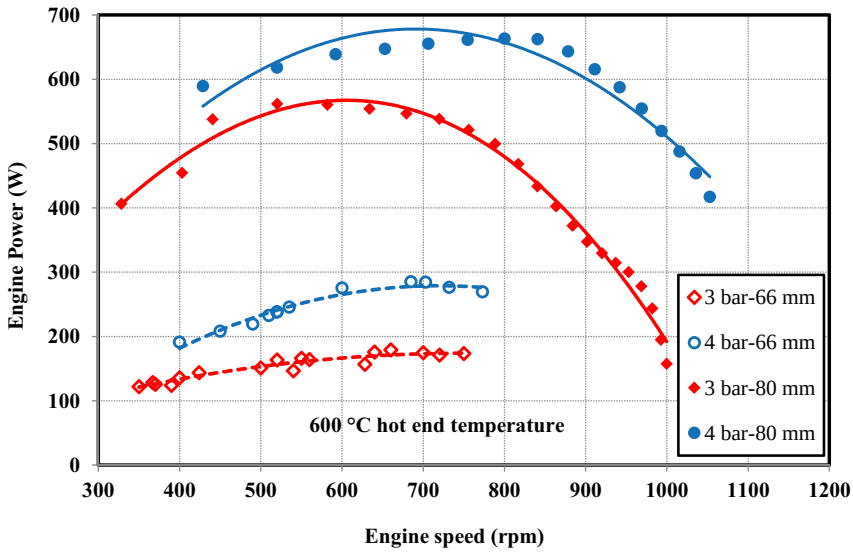

Figure 11. Variation of engine power with engine speed at 600°C.

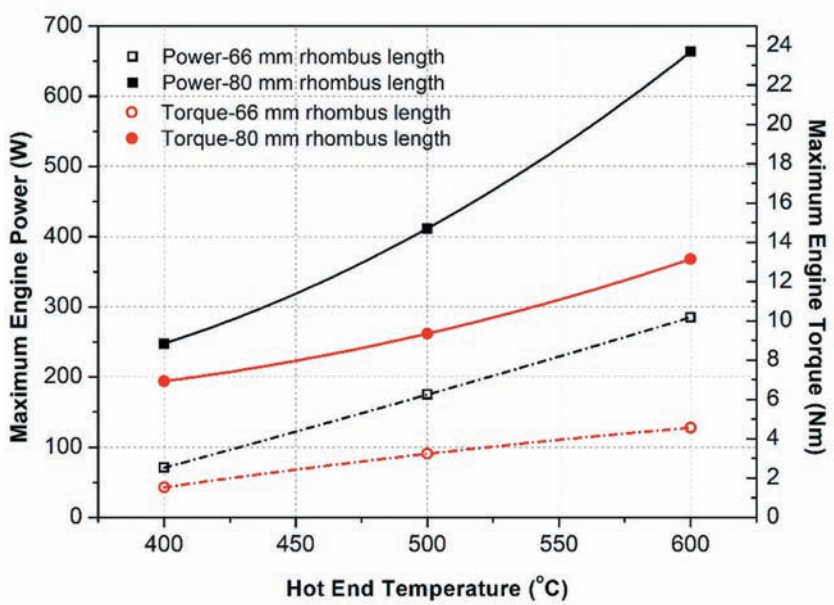

Figure 12. Variation of maximum engine torque and power versus hot-end temperature.

configurations of the engine, heat transfer areas of heater and cooler, charge pressure, type, and the mass of working fluid and regenerator volumes are same. Besides, the compression ratios of the both engine configurations are equal as 2.5. Therefore, the enhancement in engine power and torque is not related directly the thermodynamic aspects in the cylinders. It can be said that the performance enhancement in the Stirling engine was provided due to the reduced frictions in the rhombic mechanism. It should be also noted that the charge pressures of the data points on Figure 12 are not equal. At 400 °C, while the maximum torque was obtained at 2 bar charge pressure for 66 mm rhombus length arrangement, the maximum torque was obtained at a charge pressure of 3 bar for 80 mm rhombus length. In order to increase the power output of the engine at 500 and 60 °C hot end temperatures, it was determined that the charge pressure must be increased to 4 bar. The mass of working fluid increases as the charge pressure rises in the working space. At low hot end temperatures, this may cause a decrease in engine power and torque because of the insufficient heat transfer and increased compression work due to the charge mass. However, at high hot end temperatures, charge mass should be increased gradually to obtain maximum performance from the engine.

4. Conclusions

In the present study, manufacturing and testing of a beta-type Stirling engine with two different rhombic-drive mechanism were conducted. These different rhombic-

drive mechanisms were used in same beta-type Stirling engine. The main difference in the drive mechanisms are in bearings and the rod lengths. To eliminate the drawbacks of the bearing of the rhombic-drive mechanism from one side, the mechanism was supported in bearings from both sides and helical gears were used. Engine performance comparison was conducted at charge pressures of 2–4 bar and hot end temperatures of 400–600 °C by using helium as working fluid. It was found that, at a charge pressure of 4 bar and 600°C hot-end temperature, 2.88 times more engine torque was obtained as 13.14 Nm at 428 rpm for 80 mm rhombus length mechanism. The engine performance enhancement with the two sided bearing rhombic-drive mechanism was achieved due to the reduced side force acting on the crank gear and reduced frictions on the bearing. The maximum engine power was obtained as 663 W at 800 rpm engine speed at 600°C hot end temperature. The engine power increased by 132% as a result of reduced friction losses by supporting the rhombic-drive mechanism from both side and using helical gears. Gear noses were also reduced considerably.

Funding

This study was supported by TUBITAK (The Scientific and Technological Research Council of Turkey) in frame of the project code of [113M192]. As researchers, we thank to TUBITAK.

ORCID

Can Cinar http://orcid.org/0000-0001-6944-8864
Hamit Solmaz http://orcid.org/0000-0003-0689-6824
Duygu Ipci http://orcid.org/0000-0002-8862-7662
Emre Yılmaz http://orcid.org/0000-0002-5653-2079
Fatih Aksoy http://orcid.org/0000-0003-0877-9373

References

Abdullah, S., B. F. Yousif, and K. Sopian. 2005. Design consideration of low temperature differential double-acting Stirling engine for solar application. *Renewable Energy* 30 (12):1923–41.
Ahima, R. S. 2020. Global warming threatens human thermoregulation and survival. *The Journal of Clinical Investigation* 130:2.
Ahmed, F., H. Hulin, and A. M. Khan. 2019. Numerical modeling and optimization of beta-type Stirling engine. *Applied Thermal Engineering* 149:385–400.
Aksoy, F., H. Solmaz, C. Çinar, and H. Karabulut. 2017. 1.2 kW beta type Stirling engine with rhombic drive mechanism. *International Journal of Energy Research* 41 (9):1310–21.
Al Moussawi, H., F. Fardoun, and H. Louahlia-Gualous. 2016. Review of tri-generation technologies: Design evaluation, optimization, decision-making, and selection approach. *Energy Conversion and Management* 15(120):157–96.
Alfarawi, S. 2020. Thermodynamic analysis of rhombic-driven and crank-driven beta-type Stirling engines. *International Journal of Energy Research*44(7):5596-5608.
Ansari, E., K. Poorghasemi, B. K. Irdmousa, M. Shahbakhti, and J. Naber (2016). Efficiency and emissions mapping of a light duty diesel-natural gas engine operating in conventional diesel and RCCI modes. SAE Technical Paper.
Ardebili, S. M. S., H. Solmaz, and M. Mostafaei. 2019. Optimization of fusel oil–Gasoline blend ratio to enhance the performance and reduce emissions. *Applied Thermal Engineering* 148:1334–45.
Ardebili, S. M. S., A. Taghipoor, H. Solmaz, and M. Mostafaei. 2020. The effect of nano-biochar on the performance and emissions of a diesel engine fueled with fusel oil-diesel fuel. *Fuel* 268:117356.
Auguste, C., J. R. Nader, P. Marsh, and R. Cossu (2019). Influence of tidal energy converters on sediment dynamics in tidal channel.
Babaelahi, M., and H. Sayyaadi. 2016. Analytical closed-form model for predicting the power and efficiency of Stirling engines based on a comprehensive numerical model and the genetic programming. *Energy* 1 (98):324–39.
Badr, W. S., M. Fanni, A. K. Abdel-Rahman, and S. A. Rasoul. 2016. Dynamic simulation and optimization of rhombic drive Stirling engine using MSC ADAMS software. *Procedia Technology* 22:754–61.
Başaran, H. Ü. 2020. Utilizing exhaust valve opening modulation for fast warm-up of exhaust after-treatment systems on highway diesel vehicles. *International Journal of Automotive Science and Technology* 4 (1):10–22.
Bataineh, K. 2018. Mathematical formulation of alpha-type stirling engine with Ross Yoke mechanism. *Energy* 164:1178–99.
Beltrán-Chacon, R., D. Leal-Chavez, D. Sauceda, M. Pellegrini-Cervantes, and M. Borunda. 2015. Design and analysis of a dead volume control for a solar Stirling engine with induction generator. *Energy* 15 (93):2593–603.
Benato, A., and A. Stoppato. 2019. An experimental investigation of a novel low-cost photovoltaic panel active cooling system. *Energies* 12 (8):1448.
Bergquist, P., and C. Warshaw. 2019. Does global warming increase public concern about climate change? *The Journal of Politics* 81 (2):686–91.
Bosshard, P., W. Hermann, E. Hung, R. Hunt, and A. J. Simon. 2006. An assessment of solar energy conversion technologies and research opportunities. Technical Assessment Report:*GCEP Energy Assessment Analysis* 45.
Bratspies, R. 2018. Protecting the environment in an Era of Federal Retreat: The view form New York City. *FIU Law Review* 13:5.
Caetano, B. C., I. F. Lara, M. U. Borges, O. R. Sandoval, and R. M. Valle. 2019. A novel methodology on beta-type Stirling engine simulation using CFD. *Energy Conversion and Management* 184:510–20.
Calam, A. 2020. Study on the combustion characteristics of acetone/n--heptane blend and RON50 reference fuels in an HCCI engine at different compression ratios. *Fuel* 271:117646.
Calam, A., H. Solmaz, E. Yılmaz, and Y. İçingür. 2019. Investigation of effect of compression ratio on combustion and exhaust emissions in A HCCI engine. *Energy* 168:1208–16.
Can, Ö., E. Öztürk, H. Solmaz, F. Aksoy, C. Çinar, and H. S. Yücesu. 2016. Combined effects of soybean biodiesel fuel addition and EGR application on the combustion and exhaust emissions in a diesel engine. *Applied Thermal Engineering* 95:115–24.
Çelikten, İ., E. Mutlu, and H. Solmaz. 2012. Variation of performance and emission characteristics of a diesel engine fueled with diesel, rapeseed oil and hazelnut oil methyl ester blends. *Renewable Energy* 48:122–26.
Chahartaghi, M., and M. Sheykhi. 2019. Energy, environmental and economic evaluations of a CCHP system driven by Stirling engine with helium and hydrogen as working gases. *Energy*174:1251-1266
Cheng, C. H., C. Y. Huang, and H. S. Yang. 2019. Development of a 90-K beta type Stirling cooler with rhombic drive mechanism. *International Journal of Refrigeration* 98:388–98.
Cheng, C. H., and H. S. Yang. 2012. Optimization of geometrical parameters for Stirling engines based on theoretical analysis. *Applied Energy* 92:395–405.
Cheng, C. H., H. S. Yang, and L. Keong. 2013. Theoretical and experimental study of a 300-W beta-type Stirling engine. *Energy* 59:590–99.
Cheng, C. H., and Y. J. Yu. 2012. Combining dynamic and thermodynamic models for dynamic simulation of a beta-type Stirling engine with rhombic-drive mechanism. *Renewable Energy* 37 (1):161–73.
Choi, D., Z. Gao, and W. Jiang. 2020. Attention to global warming. *The Review of Financial Studies* 33 (3):1112–45.
Cinar, C. 2014. Design and manufacturing of a hermetic Stirling engine. *Proceedings of the Institution of Mechanical Engineers Part E: Journal of Process Mechanical Engineering* 228 (1):14–20.
Cinar, C., F. Aksoy, and M. Okur. 2013. Design, manufacturing and performance tests of a stirling engine with rhombic drive mechanism.

Journal of the Faculty of Engineering and Architecture of Gazi University 28 (4):795–801.
Ciniviz, M., İ. Örs, and B. S. Kul. 2017. The effect of adding EN (2-ethylhexyl nitrate) to diesel-ethanol blends on performance and exhaust emissions. *International Journal of Automotive Science and Technology* 1 (1):16–21.
Cui, Y., H. Yao, L. Hong, T. Zhang, Y. Xu, K. Xian, B. Gao, J. Qin, J. Zhang, Z. Wei, et al. 2019. Achieving over 15% efficiency in organic photovoltaic cells via copolymer design. *Advanced Materials* 31 (14):1808356.
El Tawil, T., N. Guillou, J. F. Charpentier, and M. Benbouzid. 2019. On tidal current velocity vector time series prediction: A comparative study for a French high tidal energy potential site. *Journal of Marine Science and Engineering* 7 (2):46.
Erol, D., H. Yaman, and B. Doğan. 2017. A review development of rhombic drive mechanism used in the Stirling engines. *Renewable and Sustainable Energy Reviews* 78:1044–67.
Febriansyah, B., T. M. Koh, Y. Lekina, N. F. Jamaludin, A. Bruno, R. Ganguly, Z. X. Shen, S. G. Mhaisalkar, and J. England. 2019. Improved photovoltaic efficiency and amplified photocurrent generation in mesoporous n= 1 two-dimensional lead–iodide perovskite solar cells. *Chemistry of Materials* 31 (3):890–98.
García-Gil, A., G. Goetzl, M. R. Kłonowski, S. Borovic, D. P. Boon, C. Abesser, J. Holecek. 2020. Governance of shallow geothermal energy resources. *Energy Policy* 138:111283.
Gong, J., C. Li, and M. R. Wasielewski. 2019. Advances in solar energy conversion. *Chemical Society Reviews* 48 (7):1862–64.
Gultekin, E., C. Cinar, and M. Okur. 2020. Design, manufacturing and testing of a prototype two-stroke engine with rhombic drive mechanism. *International Journal of Environmental Science and Technology* 17 (1):455–62.
Güven, M., H. Bedir, and G. Anlaş. 2019. Optimization and application of Stirling engine for waste heat recovery from a heavy-duty truck engine. *Energy Conversion and Management* 180:411–24.
Karabulut, H., H. S. Yücesu, C. Çınar, and F. Aksoy. 2009. An experimental study on the development of a β-type Stirling engine for low and moderate temperature heat sources. *Applied Energy* 86 (1):68–73.
Katopodis, T., D. Vlachogiannis, N. Politi, N. Gounaris, S. Karozis, and A. Sfetsos. 2019. Assessment of climate change impacts on wind resource characteristics and wind energy potential in Greece. *Journal of Renewable and Sustainable Energy* 11 (6):066502.
Kongtragool, B., and S. Wongwises. 2003. A review of solar-powered Stirling engines and low temperature differential Stirling engines. *Renewable and Sustainable Energy Reviews* 7 (2):131–54.
Lundie, S., T. Wiedmann, M. Welzel, and T. Busch. 2019. Global supply chains hotspots of a wind energy company. *Journal of Cleaner Production* 210:1042–50.
Ma, Q., and P. Wang. 2020. Underground solar energy storage via energy piles. *Applied Energy* 261:114361.
Masser, R., A. Khodja, M. Scheunert, K. Schwalbe, A. Fischer, R. Paul, and K. H. Hoffmann. 2020. Optimized piston motion for an alpha-type stirling engine. *Entropy* 22 (6):700.
Menegaki, A. 2008. Valuation for renewable energy: A comparative review. *Renewable and Sustainable Energy Reviews* 12 (9):2422–37.
Moulton, J. F., and J. Silverwood. 2018. On the agenda? The multiple streams of brexit-era uk climate policy. *Marmara Üniversitesi Avrupa Toplulugu Enstitüsü Avrupa Arastirmalari Dergisi* 26 (1):75–100.
Olabi, A. G., M. Mahmoud, B. Soudan, T. Wilberforce, and M. Ramadan. 2020. Geothermal based hybrid energy systems, toward eco-friendly energy approaches. *Renewable Energy* 147:2003–12.
Owusu, P. A., and S. Asumadu-Sarkodie. 2016. A review of renewable energy sources, sustainability issues and climate change mitigation. *Cogent Engineering* 3 (1):1167990.
Özsezen, A. N. 2017. Experimental analysis of performance, combustion and injection characteristics of biodiesels obtained from waste cooking and canola oils. *International Journal of Automotive Science and Technology* 1 (1):22–28.
Paulillo, A., L. Cotton, R. Law, A. Striolo, and P. Lettieri. 2020. Geothermal energy in the UK: The life-cycle environmental impacts of electricity production from the United Downs Deep Geothermal Power project. *Journal of Cleaner Production* 249:119410.
Pogulyaev, Y., O. Nikishin, and A. Zheltov. 2017. The Kinematics of the swashplate engine with two rotating pairs. *Procedia Engineering* 206:1722–27.
Polat, S., H. Solmaz, A. Uyumaz, A. Calam, E. Yilmaz, and H. S. Yucesu. 2020a. An experimental research on the effects of negative valve overlap on performance and operating range in a homogeneous charge compression ignition (HCCI) engine with RON40 and RON60 fuels. *Journal of Engineering for Gas Turbines and Power*142(5):051007
Polat, S., H. Solmaz, E. Yılmaz, A. Calam, A. Uyumaz, and H. S. Yücesu. 2020b. Mapping of an HCCI engine using negative valve overlap strategy. Energy Sources. *Part A: Recovery, Utilization, and Environmental Effects* 42 (9):1140–54.
Poorghasemi, K., R. K. Saray, E. Ansari, B. K. Irdmousa, M. Shahbakhti, and J. D. Naber. 2017. Effect of diesel injection strategies on natural gas/diesel RCCI combustion characteristics in a light duty diesel engine. *Applied Energy* 199:430–46.
Sezer, İ. 2019. A review study on the using of diethyl ether in diesel engines: Effects on HC emissions. *Avrupa Bilim Ve Teknoloji Dergisi* 16:109–24.
Shendage, D. J., S. B. Kedare, and S. L. Bapat. Jan 1, 2011. An analysis of beta type Stirling engine with rhombic drive mechanism. *Renewable Energy* 36 (1):289–97.
Solmaz, H. 2020. A comparative study on the usage of fusel oil and reference fuels in an HCCI engine at different compression ratios. *Fuel* 273:117775.
Solmaz, H., and H. Karabulut. 2014. Performance comparison of a novel configuration of beta-type Stirling engines with rhombic drive engine. *Energy Conversion and Management* 78:627–33.
Sripakagorn, A., and C. Srikam. 2011. Design and performance of a moderate temperature difference Stirling engine. *Renewable Energy* 36 (6):1728–33.
Teo, H. G., P. S. Lee, and M. N. Hawlader. 2012. An active cooling system for photovoltaic modules. *Applied Energy* 90 (1):309–15.
Tilley, S. D. 2019. Recent advances and emerging trends in photo-electrochemical solar energy conversion. *Advanced Energy Materials* 9 (2):1802877.
Uyumaz, A. 2020. Experimental evaluation of linseed oil biodiesel/diesel fuel blends on combustion, performance and emission characteristics in a DI diesel engine. *Fuel* 267:117150.
Uyumaz, A., F. Aksoy, F. Boz, and E. Yılmaz. 2017. Experimental investigation of neutralized waste cooking oil biodiesel and diesel fuels in a direct injection diesel engine at different engine loads. *International Journal of Automotive Science and Technology* 1 (1):7–15.
Wang, J., S. Zhou, Z. Zhang, and D. Yurchenko. 2019. High-performance piezoelectric wind energy harvester with Y-shaped attachments. *Energy Conversion and Management* 181:645–52.
Wang, K., S. R. Sanders, S. Dubey, F. H. Choo, and F. Duan. 2016. Stirling cycle engines for recovering low and moderate temperature heat: A review. *Renewable and Sustainable Energy Reviews* 62:89–108.
Wigley, T. M. 2018. The Paris warming targets: Emissions requirements and sea level consequences. *Climatic Change* 147 (1–2):31–45.
Wigley, T. M. L., L. E. Clarke, J. A. Edmonds, H. D. Jacoby, S. Paltsev, H. Pitcher, J. M. Reilly, R. Richels, M. C. Sarofim, and S. J. Smith. 2009. Uncertainties in climate stabilization. *Climatic Change* 97 (1–2):85.
Yang, H. S., C. H. Cheng, and S. T. Huang. 2018. A complete model for dynamic simulation of a 1-kW class beta-type Stirling engine with rhombic-drive mechanism. *Energy* 161:892–906.